IEEE Photonics Journal
An IEEE Photonics Society Publication

Open Access

High-Sensitive Refractive Index Sensing Enabled by Topological Charge Evolution

Volume 12, Number 5, October 2020

Jiaxin Lv
Zihao Chen
Xuefan Yin
Zixuan Zhang
Weiwei Hu
Chao Peng

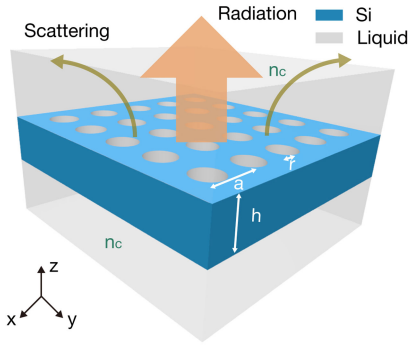

DOI: 10.1109/JPHOT.2020.3017806

High-Sensitive Refractive Index Sensing Enabled by Topological Charge Evolution

Jiaxin Lv, Zihao Chen, Xuefan Yin, Zixuan Zhang, Weiwei Hu, and Chao Peng

State Key Laboratory of Advanced Optical Communication Systems and Networks, Department of Electronics, Peking University, Beijing 100871, China

DOI:10.1109/JPHOT.2020.3017806

Manuscript received June 18, 2020; revised August 13, 2020; accepted August 16, 2020. Date of publication August 19, 2020; date of current version September 14, 2020. This work was supported in part by the National Key Research and the Development Project of China under Grant 2018YFB2201704, in part by the National Natural Science Foundation of China under Grant 61922004, and in part by the State Key Laboratory of Advanced Optical Communication Systems and Networks, China. Corresponding author: Chao Peng (e-mail: pengchao@pku.edu.cn).

Abstract: A high-sensitive refractive index sensor is proposed and demonstrated by utilizing merging bound states in the continuum, namely a set of integer topological charges in the momentum space. Through varying cladding refractive index n_c, the topological charges continuously depart from the merging state, and result in the robust and considerable high-Q factors (above 7×10^4) in a large detection range of 0.456. In such a range, sensing sensitivity of $\sim$36 nm/RIU and figure-of-merit from $\sim$5990 (air) to 1607 ($n_c = 1.456$) are achieved. Meanwhile, the detection limit on the order of 10^{-5} RIU is clearly distinguishable from the measured spectrum under tiny variation of cladding refractive index. Our work paves the way for promising integrated high-sensitive sensors in many biological and chemical applications.

Index Terms: Photonic crystal, optical sensor, high-Q resonance, topological charge, bound state in the continuum.

1. Introduction

Refractive index (RI) depicts the speed of light that propagates in the material. Many physical processes, such as current injection, temperature variation, chemical reaction, biological activity, would result in modifying the refractive index. Hence, sensing such small refractive index change is important and valuable for many biological and chemical applications [1]–[3] arranged from disease diagnosis, environment monitoring, to chemical/gas analysis. Among many RI sensors, the optical resonators [4], [5] have attracted widespread attention. In these sensors, the refractive index change is monitored by precisely measuring the wavelength shift of optical resonance, which enables promising features of high-sensitive and label-free.

To sense tiny surrounding medium change, the figure-of-merit (FOM) and the detection limit (DL) are two important attributes for characterizing RI sensor performance [6]. The FOM takes into account the sharpness of resonance, namely the quality-factor Q, and the sensor's sensitivity S as well [7], defined as FOM $= S/\text{FWHM}$, where FWHM is the full width at half-maximum of optical resonance. On the other hand, the DL represents a lower bound on the detectable refractive index change [8], which is defined as DL $= R/S$, where R is the minimal distinguishable wavelength shift, which is conventionally set as 1/20th of the spectral line-width that can be clearly distinguishable [8]–[10]. Therefore, both high Q and high sensitivity help achieve a lower detection limit [9].

From such relations, we readily find that high-Q resonances are always beneficial. Indeed, many high-Q resonators, including photonic crystal cavities (PhC) [11], [12], micro-ring resonators [13], [14], whispering gallery mode cavities [15], [16], etc., have been explored for building compact on-chip integrated RI sensors. For PhC devices, localized PhC defect cavities [17]–[20] offer a moderately high Q of $10^4 \sim 10^5$, but small field overlap with the analyte limits their sensitivities. The slotted PhC cavities [21]–[25] can achieve higher sensitivity by increasing the mode field overlap with the analyte, but they are quite fragile to fabrication imperfections and Qs are conventionally limited to $10^3 \sim 10^4$ in experiment. Besides, another major drawback of above mentioned sensors is that they require delicate alignment in order to couple the light from free space to the device, which brings more losses and complexities.

PhC based on guided mode resonance (GMR) provides another promising approach for RI sensing [26], [27]. Such devices are defect-free and easy-to-fabrication. Besides, GMR can be excited from surface-normal incidence that relaxes the alignment constraints of coupling. The theoretical Qs of GMRs are infinite at normal incident angle ($k = 0$), which are also known as the bound states in the continuum (BICs) - discrete states with infinite lifetime even out-going waves are allowed. A series of pioneering works had demonstrated BIC-based RI sensors [28] upon silicon-on-insulator (SOI) [9], [29]–[31] and silicon nitride platforms [6], [12], [26], [32], [33]. By exiting at small incident angle ($k \approx 0$), the Qs about $1 \sim 3 \times 10^4$ had been achieved and resulted in DL up to $3 \sim 6 \times 10^{-5}$ RIU in experiments [9], [29].

Besides the reported advances, we believe the BIC-based RI sensors still have huge potentials to be improved, since the Qs of BICs in PhC are infinite in theory [34]–[44]. However, the observed Qs of BICs degrade a lot in realistic devices. The losses come from many aspects, in which the material absorption and out-of-plane scatterings are dominant. For RI sensors, the material absorption can be avoided by appropriately choosing analyte solvent. While the out-of-plane scatterings, which origin from the random fluctuations induced by fabrication imperfections, are practically inevitable.

Recently, we reported a novel approach of suppressing out-of-plane scatterings in PhC and the Qs as high as 4.9×10^5 had been experimentally achieved in SOI platform [45]. It is found that the fundamental nature of BICs in PhC slabs is topological [46], [47]: they are essentially topological defects of polarization directions defined in the momentum space, known as non-trivial topological charges. Further, by manipulating a set of the topological charges merging at the Brillouin zone (BZ) center that we named as merging BICs, the optical resonances become more robust to out-of-plane scatterings, which is the dominant practically inevitable reason of Q degrading.

In this work, we propose to adopt merging BICs in RI sensing, by utilizing the robust high-Q nature to promote the FOM and DL performances. Specifically, we immerse the PhC sample in a series of liquids with calibrated increments of refractive index n_c from 1.300 to 1.456, then measure the wavelength of high-Q resonance λ_0 accordingly and find the dependence $\lambda_0(n_c)$. From topological point of view, varying the refractive index of upper/lower cladding (n_c) is also equivalent to make the topological charges continuously depart from the merging state. Owing to the robustness of merging BICs, the Qs constantly keep higher than 7×10^4 when n_c varying from 1.000 (air) to 1.456 (liquid). In such a range, sensing sensitivity S of $\sim$36 nm/RIU and FOM from $\sim$5990 (air) to 1607 ($n_c = 1.456$) are guaranteed. Meanwhile, the ultimate detection limit represented by the 1/20th of resonance line-width is estimated as 10^{-5} RIU from the measured spectrum.

The remainder of this paper is organized as follows. Section 2 describes the theory and principle of using merging BICs for RI sensing. Section 3 presents the fabrication process of the PhC samples upon SOI wafer and the measurement setup for the characterization at 1.5 μm wavelength. Section 4 summarizes the experiment results and presents some discussion on sensitivity performance. Finally, we conclude our work in Section 5.

2. Theory and Principle

The schematic of PhC for refractive index sensing is illustrated in the left panel of Fig. 1(a), in which a two-dimensional (2D) PhC is patterned on a silicon-on-insulator (SOI) wafer with silicon layer thickness of $h = 600$ nm. The PhC consists of a series of holes (radius $r = 171.9$ nm) upon square

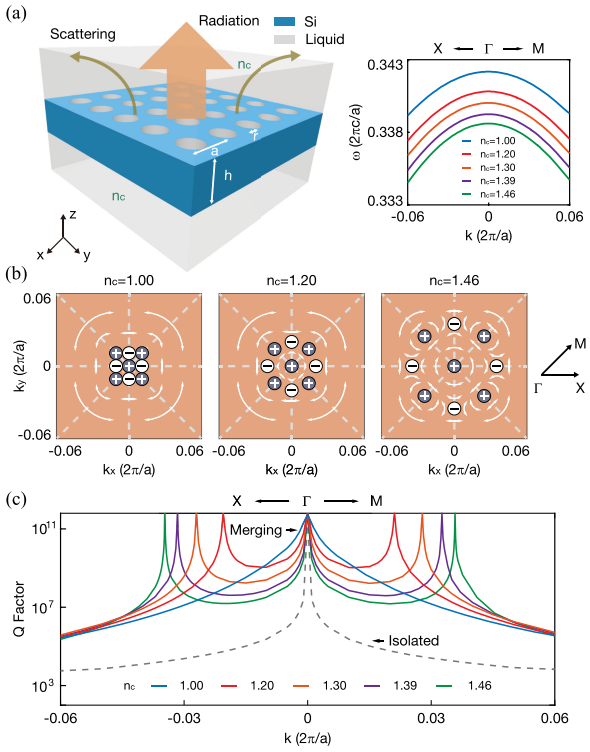

Fig. 1. Refractive index sensing accompanied with topological charge evolution. (a) Left, schematic of PhC for refractive index sensing. Right, simulated band structures of TE-like mode with different cladding refractive index n_c. (b) Nine BICs with topological charges ± 1 merging at the center of BZ (left), depart from each other (mid/right), as n_c varying. (c) High and robust Qs maintain in a wide detection range Δn_R. Simulated Qs originating from merging BICs design (solid lines) for different n_c, robustly higher than the isolated BIC configuration (dashed line). All simulations used COMSOL.

lattice (periodicity $a = 531.42$ nm). The system owns mirror-symmetry in the vertical direction (σ_z) and operates upon the lowest TE-like band (E_x, E_y, H_z) in the continuum (Fig. 1(a), right panel). As we elaborated in our previous work [45], the theoretical lifetime of optical resonances goes to infinity at 9 discrete k points in the momentum space thus exhibited as 9 BICs: one is pinned at the Brillouin zone (BZ) center owing to symmetry protection, while the rest of eight are tunable due to weighted destructive interference that cancels out all of the radiations.

However, other than the vanishing of radiation through interference, a more common and physical interpretation underlying the BICs has been identified to be topological: they are essentially topological defects in the momentum space, namely non-trivial topological charges (q), defined as the winding numbers of polarization vector field with given state, as:

$$q = \frac{1}{2\pi} \oint_C d\mathbf{k} \cdot \nabla_{\mathbf{k}} \theta(\mathbf{k}) \tag{1}$$

Here, $\theta(\mathbf{k}) = \arg[c_x(\mathbf{k}) + ic_y(\mathbf{k})]$ is the angle of polarization vector that depicting the radiation field $\phi(\mathbf{k}) = c_x\hat{x} + c_y\hat{y}$ and C is a closed simple path in the momentum space that going around the state in the counterclockwise (CCW) direction. From this point of view, the BICs are vortices of polarization vector in the momentum space, represented by integer topological charges of $q \in Z$, as shown in Fig. 1(b). At the vortices center, the polarization of radiation can not be defined and thus the radiation itself can not exist, which is exactly the BIC.

It is noteworthy that: topological charges cannot suddenly disappear, because they are conserved and quantized quantities - they could continuously evolve in the momentum space; unless one drops out of the light cone, or annihilates with an exact opposite topological charge carried by another BIC. In our previous work [45], we manipulate the topological charges gradually moving

and merging towards the BZ center in the momentum space, by varying the lattice periodicity a - we refer to this design as "merging BICs". The merging of topological charges leads to non-trivial consequence: the scaling rules of energy radiation then are modified to k^6 from conventional k^2 dependency, in which k is the momentum distance away from the Γ point. As a result, the Qs of all resonances nearby the BZ center are enhanced thus less susceptible to out-of-plane scatterings. Q as high as 4.9×10^5 has been observed based on these resonances in the telecommunication regime, which is 12-times higher than ordinary isolated BIC designs.

From topological point of view, we can choose an alternative structure or material parameter other than lattice periodicity a to control the topological charge evolution. In this work, we choose the varying parameter to be the cladding refractive index n_c, which is also the target for RI sensing. As shown in the right of Fig. 1(a) (COMSOL, Multiphysics), when n_c varies from 1.00 to 1.46, the resonance frequencies shift accordingly. At the same time, the topological charges gradually depart from the merging state (Fig. 1(b), left panel), to the outer of BZ region (Fig. 1(b), mid/right panels). However, owing to the robustness of topological charges, theoretical infinite lifetime of BICs maintains at given k points (Fig. 1(b)). And importantly, the robustness to random out-of-plane scatterings also remains in a certain degree, because the modified scaling rule still approximately holds when the topological charges are not moving far away from the merging state.

The high-Q nature discussed above offers a promising feature for the RI sensing. In conventional RI sensors based on optical resonances, the change of RI would break the condition of ideal destructive interference and result in degrading of Qs, and thus limits the sensors' FOM/DL performances. In Fig. 1(c), the proposed design remains high and robust Qs in a wide range of RI change, even in the existence of random scattering losses that are inevitable due to the fabrication imperfections in practical samples. Thus, the simulated Qs originating from merging BICs design at different n_c are robustly higher than the isolated BIC configuration (periodicity a $=$ 580 nm).

3. Sample Fabrication and Measurement Setup

To verify the proposed sensing principle, we fabricated PhC samples in which the topological charges are designed to be merging at BZ center for an air-bridged cladding ($n_c = 1$). The PhCs are on 600-nm-thick silicon-on-insulator (SOI) wafer with footprints of 266 μm $\times$ 266 μm. The samples are fabricated by using electron-beam lithography (EBL) and inductively coupled plasma (ICP) dry etching. In order to achieve up-down mirror symmetry, we removed the underlying SiO_2 layer by utilizing hydrofluoric acid (HF) undercutting. The scanning electron microscope (SEM) images of fabricated sample are shown in the Fig. 2(b),(c).

We characterize the high-Q resonances by using the measurement setup schematically illustrated in Fig. 2(a). Firstly, an incident light is generated from a tunable laser (Santec, TSL-550) in the telecommunication wavelength of 1550 nm, and the incident wavelength can be swept in high precision. After collimation, the incidence goes through the beam splitter (BS) and then focuses on the sample by an objective lens (Mitutoyo, NA $=$ 0.26). Then, reflected light is collected by the objective lens and sent through two relay 4f systems, with magnification ratio of 1.33. Finally, reflected light can be detected by photodetector (PD, Thorlabs, PDA10PT) to measure reflection spectra of high-Q resonances. By using a pin-hole located at the Fourier imaging plane, the radiation at desired k wavevector is picked out. In order to achieve better signal to noise ratio (SNR), a cross-polarization technique is applied. For more details of the setup, please refer to our previous work [45].

To modify the refractive index of PhC cladding n_c, we immerse the sample into a container that is filled with refractive-index-matching liquids with n_c from 1.300 to 1.456 (Cargille, A series). Note that the up-down mirror symmetry consistently maintains during the test. We shield the liquid container to our best to avoid the influence of air flow and temperature variation in the surroundings. Besides, a temperature sensor is continuously monitoring the liquid temperature for later calibration. We use pipettes to replace refractive-index-matching liquids. Given the liquid volume of single pipette drop is nearly constant (0.05 ml), we count the same number of drops to assure repeatability.

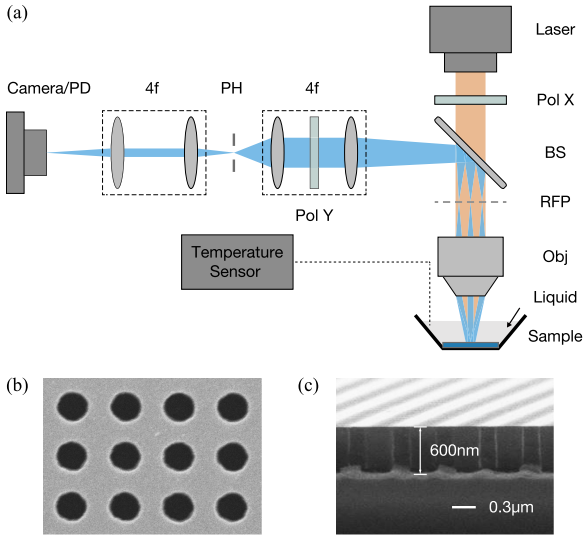

Fig. 2. Experimental Setup. (a) Schematic of the measurement setup for refractive index sensing. Orange line represents the incident light focusing on the sample. Blue line is reflected light which is collected by two cascaded 4f systems and detected by a photodetector. The sample is immersed in refractive-index-matching liquids and the temperature is monitored with a temperature sensor. Pol X, polarizer along x-axis. BS, beam splitter. RFP, rear focal plane. Obj, objective lens. Pol Y, polarizer along y-axis. PH, pin hole. PD, photodetector. (b)–(c) Scanning electron microscope images of the fabricated PhC sample, from top and side views.

4. Results and Discussion

As mentioned, the FOM of refractive index sensor highly depends on the line-width, namely the Q of optical resonance. As presented in Fig. 3(a), for the sample we tested in this work, optical resonances possess considerably high Qs under varying cladding refractive index n_c, which exhibited as Fano line-shapes because of the existence of residual reflections under refractive-index mismatching between the liquid and air. The Qs of optical resonances are extracted by fitting the Fano line-shapes and the quantitative results are demonstrated in Fig. 3(b). The Q up to $\sim 2.6 \times 10^5$ is observed for air cladding ($n_c = 1$) and keeps consistently higher than $\sim 7.0 \times 10^4$ when n_c varying from 1.300 to 1.456. All of the observations are performed at fixed k-point of $k_x a/2\pi = 0.006$, $k_y a/2\pi = 0.006$. The fabricated samples would inevitably deviate from their ideal designs due to fabrication imperfections, and lead to considerably degrading of radiative Qs. We applied an asymmetric shape to represent typical fabrication errors with tilted angle $\theta = \sim 2^\circ$ and center shift of $\Delta x = 2$ nm, $\Delta y = 4$ nm that are extracted from SEM observations, and further calculated the radiative Qs similar to our previous work [45]. As illustrated in Fig. 3(b), the simulated Qs agree with the experiments in the order of magnitude, and the slight difference between them may originate from those non-radiative processes [43], including the wafer roughness, structural disorder, material absorption and lateral leakage. As shown in Fig. 3(c), at the room temperature (25 °C), the measured resonance peaks red shift from 1562.20 nm to 1567.78 nm, which agrees well with numerical simulations and proves the linear dependence between the resonance peak λ_0 and the cladding refractive index n_c.

The sensitivity is given as $S = \Delta\lambda_0/\Delta n_c$, where $\Delta\lambda_0$ is the shift of characteristic wavelength peak and Δn_c is the refractive index change of surrounding dielectric medium. Thus, the sensing sensitivity is estimated as ~36 nm/RIU in large n_c ranges. On the other hand, the FOM that is defined as FOM $= S/$FWHM, is from ~5990 (air) to 1607 ($n_c = 1.456$). Therefore, we found that the detection range of proposed sensor can be as wide as $\Delta n_R = 0.456$ without scarifying the sensitivity and FOM performances too much.

In order to show the capability of detecting ultra-small refractive index change, we perform a fine measurement of optical resonances shifting for given cladding refractive index n_c near 1.345. To

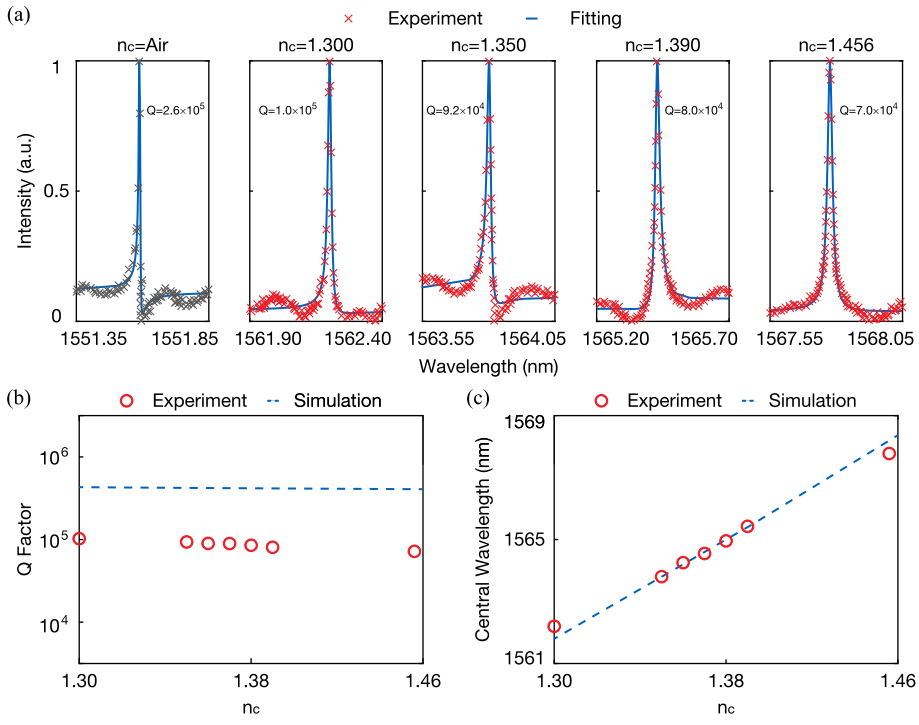

Fig. 3. Performance of refractive index sensing in large n_c ranges. (a) Measured spectrums of high-Q resonances for different n_c. The intensities characterized by photodetector (markers) are fitted with Fano line-shapes (lines) as a function of wavelengths. (b) The Q-factors versus n_c, including the measurement results (circles) and the simulations with fabrication errors (dashed line). (c) Central resonance wavelengths red shift as n_c tuning from 1.300 to 1.456. The experimental results (circles) show good agreement with numerical simulations (dashed line).

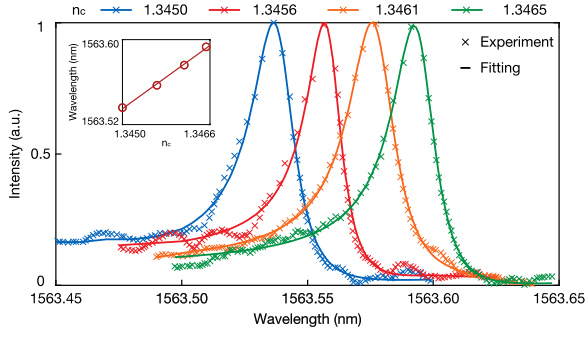

Fig. 4. High resolution refractive index sensing. Refractive index change as small as $\Delta n_c = 10^{-4}$ is detected and resonance peak almost shifts a wavelength of FWHM from high-Q resonance each measure. The small Δn_c is obtained from the volume-mixtures of two refractive-index-matching liquids ($n_c = 1.345$ and $n_c = 1.350$). Inset: central resonance wavelengths slightly shift as a function of n_c with the temperature compensation.

obtain tiny tuning n_c, we firstly fill 70 drops of refractive-index-matching liquids with $n_c = 1.345$ into the container by using pipette, which establishes the initial environment. Next, we progressively add 10 drops of liquids each time ($n_c = 1.350$) to make tiny increment of refractive index; meanwhile, measure the reflection spectrums simultaneously and record the temperature for later calibration. As illustrated in Fig. 4, the resonance peaks are distinguishable for each measure, which are almost separated by a wavelength of FWHM from the high-Q resonances through applying every 10 drops. The inset in Fig. 4 shows the wavelength dependencies upon n_c, which are calculated from

volume-mixtures of two refractive-index-matching liquids ($n_c = 1.345$ and 1.350) and calibrated with temperature. The data reveals that, the proposed sensor is capable of detecting refractive index change as small as $\Delta n_c = 10^{-4}$. The sensitivity of ~38 nm/RIU and FOM of ~2235 are obtained here, showing good agreement with the large-range measuring of Fig. 3. From such results, when the 1/20th line-width of optical resonance is set as minimal wavelength shift R that can be easily distinguished from the measured resonance spectrum, thus the DL is on the order of 10^{-5} RIU.

It is noteworthy to discuss the temperature stability of proposed sensor. As shown in Fig. 4, owing to the ultra-high-Q nature of merging BICs design, the refractive index change $\Delta n_c = 10^{-4}$ is detected, which makes a line-width shift of characteristic resonance peak $\Delta\lambda_0 = \sim 0.017$ nm. We estimate from the thermo-optic coefficient of silicon ($dn/dT = 1.86 \times 10^{-4} K^{-1}$), which gives $\Delta\lambda_t = 0.018$ nm when temperature variation of $\Delta T = 1\ ^\circ$C. Monitored from the embedded temperature sensor, the temperature variation during our test period is about 0.1 °C, which indicates temperature compensation is necessary.

We summarize the device parameters and sensing performances as the table shown in Appendix. Owing to the ultra-high-Q resonance and fabrication-robust features of merging BICs design, the proposed RI sensor shows improvement in FOM, with ~5990 (air) / 1607 ($n_c = 1.456$) and lower DL of 2.2×10^{-5} RIU ($R = 1/20 \times$ FWHM, $n_c = 1.300$, $k_x a/2\pi = 0.006$, $k_y a/2\pi = 0.006$), when comparing with the reported works in which conventional isolated BIC is adopted [6], [9], [29], [32]. Given that the merging BICs offer almost one order of magnitude higher Qs than the isolated BIC can achieve, the promotion of FOM/DL performance seems not so exciting as expected. The reason is the sensitivity of current merging BICs design is only ~36 nm/RIU, which is lower than the reported results as ~100 nm/RIU [9], [29].

Therefore, it is noteworthy to discuss the sensitivity of merging BICs design. As elaborated in Ref [12], [26], the sensitivity depends on the overlap integral f as the ratio of electric field energy in the analyte region to the total energy for a given mode:

$$f = \frac{\int_{V_{\text{analyte}}} \varepsilon |E|^2 dV}{\int_{V_{\text{total}}} \varepsilon |E|^2 dV} \tag{2}$$

where ε is the permittivity of materials. Then the sensitivity S is proportional to f, as

$$S = \frac{\Delta\lambda_0}{\Delta n_{\text{analyte}}} = \lambda_0 \frac{f}{n_{\text{analyte}}} \tag{3}$$

Because thick SOI wafer (600 nm) is adopted in current merging BICs design, the overlap ratio f is 3.2% that is smaller than the reported of isolated BIC design [29].

There are several ways to promote the sensitivity performance, including using lower-refractive-index contrast material (such as Si_3N_4), using thinner wafer slab to weaken the guided-mode confinement, as well as adopting TM-like modes rather than TE-like modes [26]. As shown in Fig. 5, the isolated BIC on TM-band offers $f = 70.9\%$ and $S = 815$ nm/RIU in simulation [9], because the modal electric field E_z overlaps more with the analyte than its TE counterpart (E_x, E_y). We argue that, using merging BICs to promote practical Qs is a general principle that is also valid for TM-band, high-order-Γs, as well as different materials. Therefore, the sensitivity is not the fundamental limitation of applying merging BICs for RI sensors.

5. Conclusion

In this work, we propose and demonstrate a type of refractive index sensor by adopting ultra-high-Q and robust fabrication optical resonance in photonic crystal slab based on SOI platform. The high-Q resonance originates from merging a set of BICs, namely topological charges in the momentum space, towards the center of Brillouin zone: we refer to it as “merging BICs design”. We show that, other than lattice periodicity, the topological charges also evolve with the varying cladding refractive index n_c. In this case, the Qs of optical resonances remain considerably high (above 7.0×10^4) in varying n_c ranges from 1.000 (air) to 1.456 (liquid). As a result, the proposed sensor is capable

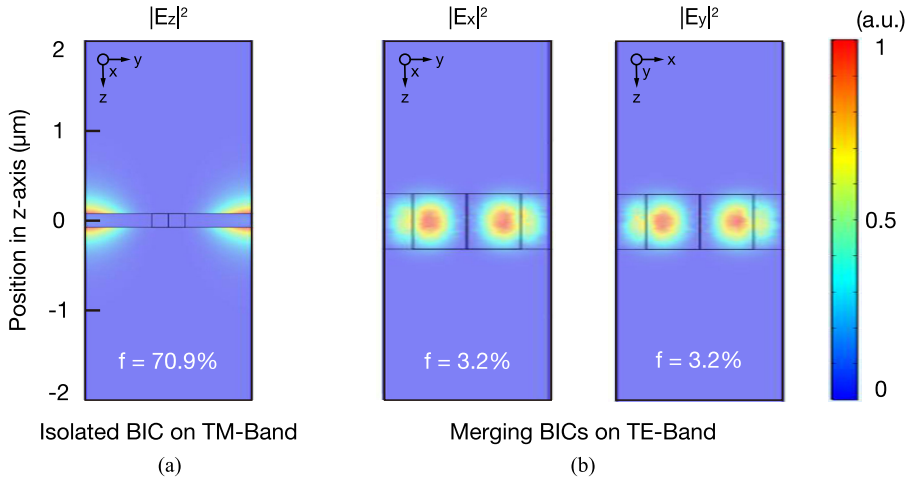

Fig. 5. Mode profile on different bands. (a) Simulated electric-field energy distribution of the isolated BIC on TM-band (a = 1000 nm, r = 100 nm, h = 160 nm, $k_x a/2\pi = 10^{-4}$) [9]. (b) Simulated electric-field energy distribution of the merging BICs on TE-band in our work (a = 531.42 nm, r = 171.9 nm, h = 600 nm, $k_x a/2\pi = 10^{-4}$).

of large detection range $\Delta n_R = 0.456$, and in such a range, sensing sensitivity of ~36 nm/RIU and FOM from ~5990 (air) to 1607 ($n_c = 1.456$) are achieved. Meanwhile, through fine tuning the refractive index and compensating the temperature variation, the refractive index change on the order of 10^{-4} is detected. When the system resolution R is set as the 1/20th of spectral line-width, the detection limit is on the order of 10^{-5} RIU which is clearly distinguishable from the measured spectrum. The proposed sensor shows excellent performances of figure-of-merit, detection limit as well as detection range, thus could be promising as integrated refractive index sensor for many biological and chemical applications arranged from disease diagnosis, environment monitoring, to chemical/gas analysis.

Appendix: Device Parameters and Sensing Performances

	Parameter	Value
Structure	Periodicity	531.42 nm
	Radius	171.9 nm
	Duty cycle	0.33
	Thickness	600 nm
	Footprint	266 μm × 266 μm
Simulation ($k_x a/2\pi$=10^{-4}, n_c=1.300)	Sensitivity	38 nm/RIU
	Quality-factor	1.6×10^{11}
	Figure of merit	3.9×10^{9}
	Detection limit	1.3×10^{-11} RIU
Experiment (n_c=1.300)	Sensitivity	36 nm/RIU
	Quality-factor	1.0×10^{5}
	Figure of merit	2.3×10^{3}
	Detection limit	2.2×10^{-5} RIU

References

[1] S. Wang, Y. Liu, D. Zhao, H. Yang, W. Zhou, and Y. Sun, "Optofluidic fano resonance photonic crystal refractometric sensors," *Appl. Phys. Lett.*, vol. 110, no. 9, 2017, Art. no. 091105.

[2] L. Wang *et al.*, "A label-free optical biosensor built on a low-cost polymer platform," *IEEE Photon. J.*, vol. 4, no. 3, Jun. 2012.

[3] X. Fan, I. M. White, S. I. Shopova, H. Zhu, J. D. Suter, and Y. Sun, "Sensitive optical biosensors for unlabeled targets: A review," *Analytica Chimica Acta*, vol. 620, no. 1, pp. 8–26, 2008.

[4] B. Cunningham, B. Lin, J. Qiu, P. Li, J. Pepper, and B. Hugh, "A plastic colorimetric resonant optical biosensor for multiparallel detection of label-free biochemical interactions," *Sensors Actuators B: Chem.*, vol. 85, no. 3, pp. 219–226, 2002.

[5] R. Magnusson, D. Wawro, S. Zimmerman, and Y. Ding, "Resonant photonic biosensors with polarization-based multiparametric discrimination in each channel," *Sensors*, vol. 11, no. 2, pp. 1476–1488, 2011.

[6] S. Romano *et al.*, "Label-free sensing of ultralow-weight molecules with all-dielectric metasurfaces supporting bound states in the continuum," *Photon. Res.*, vol. 6, no. 7, pp. 726–733, 2018.

[7] A. V. Kabashin *et al.*, "Plasmonic nanorod metamaterials for biosensing," *Nat. Mater.*, vol. 8, no. 11, pp. 867–871, 2009.

[8] I. M. White and X. Fan, "On the performance quantification of resonant refractive index sensors," *Opt. Express*, vol. 16, no. 2, pp. 1020–1028, 2008.

[9] Y. Liu, W. Zhou, and Y. Sun, "Optical refractive index sensing based on high-q bound states in the continuum in free-space coupled photonic crystal slabs," *Sensors*, vol. 17, no. 8, 2017, Art. no. 1861.

[10] S. Arnold, M. Khoshsima, I. Teraoka, S. Holler, and F. Vollmer, "Shift of whispering-gallery modes in microspheres by protein adsorption," *Opt. Lett.*, vol. 28, no. 4, pp. 272–274, 2003.

[11] M. Huang, A. A. Yanik, T. Y. Chang, and H. Altug, "Sub-wavelength nanofluidics in photonic crystal sensors," *Opt. Express*, vol. 17, no. 26, pp. 24 224–24 233, 2009.

[12] C. Nicolaou, W. T. Lau, R. Gad, H. Akhavan, R. Schilling, and O. Levi, "Enhanced detection limit by dark mode perturbation in 2D photonic crystal slab refractive index sensors," *Opt. Express*, vol. 21, no. 25, pp. 31 698–31 712, 2013.

[13] Y. Sun and X. Fan, "Analysis of ring resonators for chemical vapor sensor development," *Opt. Express*, vol. 16, no. 14, pp. 10 254–10 268, 2008.

[14] X. Tu, S. L. Chen, C. Song, T. Huang, and L. J. Guo, "Ultrahigh q polymer microring resonators for biosensing applications," *IEEE Photon. J.*, vol. 11, no. 2, Apr. 2019, Art. no. 4200110.

[15] F. Vollmer and S. Arnold, "Whispering-gallery-mode biosensing: Label-free detection down to single molecules," *Nature Methods*, vol. 5, no. 7, pp. 591–596, 2008.

[16] Y. F. Xiao *et al.*, "High-q exterior whispering-gallery modes in a metal-coated microresonator," *Physical Rev. Lett.*, vol. 105, no. 15, 2010, Art. no. 153902.

[17] D. Dorfner *et al.*, "Photonic crystal nanostructures for optical biosensing applications," *Biosensors Bioelectronics*, vol. 24, no. 12, pp. 3688–3692, 2009.

[18] W. C. Lai, S. Chakravarty, Y. Zou, Y. Guo, and R. T. Chen, "Slow light enhanced sensitivity of resonance modes in photonic crystal biosensors," *Appl. Phys. Lett.*, vol. 102, no. 4, 2013, Art. no. 041111.

[19] C. Kang, C. T. Phare, Y. A. Vlasov, S. Assefa, and S. M. Weiss, "Photonic crystal slab sensor with enhanced surface area," *Opt. Express*, vol. 18, no. 26, pp. 27 930–27 937, 2010.

[20] M. Lee and P. M. Fauchet, "Two-dimensional silicon photonic crystal based biosensing platform for protein detection," *Opt. Express*, vol. 15, no. 8, pp. 4530–4535, 2007.

[21] B. Wang, M. A. Dündar, R. Nötzel, F. Karouta, S. He, and R. W. van der Heijden, "Photonic crystal slot nanobeam slow light waveguides for refractive index sensing," *Appl. Phys. Lett.*, vol. 97, no. 15, 2010, Art. no. 151105.

[22] D. Yang *et al.*, "High sensitivity and high q-factor nanoslotted parallel quadrabeam photonic crystal cavity for real-time and label-free sensing," *Appl. Phys. Lett.*, vol. 105, no. 6, 2014, Art. no. 063118.

[23] M. G. Scullion, A. D. Falco, and T. F. Krauss, "Slotted photonic crystal cavities with integrated microfluidics for biosensing applications," *Biosensors Bioelectronics*, vol. 27, no. 1, pp. 101–105, 2011.

[24] A. Di Falco, L. O'Faolain, and T. F. Krauss, "Chemical sensing in slotted photonic crystal heterostructure cavities," *Appl. Phys. Lett.*, vol. 94, no. 6, 2009, Art. no. 063503.

[25] D. Yang, H. Tian, Y. Ji, and Q. Quan, "Design of simultaneous high-q and high-sensitivity photonic crystal refractive index sensors," *J. Opt. Soc. Amer. B*, vol. 30, no. 8, pp. 2027–2031, 2013.

[26] M. E. Beheiry, V. Liu, S. Fan, and O. Levi, "Sensitivity enhancement in photonic crystal slab biosensors," *Opt. Express*, vol. 18, no. 22, pp. 22 702–22 714, 2010.

[27] S. Fan and J. D. Joannopoulos, "Analysis of guided resonances in photonic crystal slabs," *Physical Rev. B*, vol. 65, no. 23, 2002, Art. no. 235112.

[28] R. Gansch *et al.*, "Measurement of bound states in the continuum by a detector embedded in a photonic crystal," *Light: Sci. Appl.*, vol. 5, no. 9, 2016, Art. no. 16147.

[29] Y. Liu, S. Wang, D. Zhao, W. Zhou, and Y. Sun, "High quality factor photonic crystal filter at k $\approx$ 0 and its application for refractive index sensing," *Opt. Express*, vol. 25, no. 9, pp. 10 536–10 545, 2017.

[30] F. Yesilkoy *et al.*, "Ultrasensitive hyperspectral imaging and biodetection enabled by dielectric metasurfaces," *Nature Photon.*, vol. 13, no. 6, pp. 390–396, 2019.

[31] Y. Liu, S. Wang, P. Biswas, P. Palit, W. Zhou, and Y. Sun, "Optofluidic vapor sensing with free-space coupled 2D photonic crystal slabs," *Scientific Rep.*, vol. 9, no. 1, 2019, Art. no. 4209.

[32] S. Romano *et al.*, "Tuning the exponential sensitivity of a bound-state-in-continuum optical sensor," *Opt. Express*, vol. 27, no. 13, pp. 18 776–18 786, 2019.

[33] S. Romano *et al.*, "Optical biosensors based on photonic crystals supporting bound states in the continuum," *Materials*, vol. 11, no. 4, 2018, Art. no. 526.

[34] C. W. Hsu, B. Zhen, A. D. Stone, J. D. Joannopoulos, and M. Soljačić, "Bound states in the continuum," *Nature Rev. Mater.*, vol. 1, no. 9, pp. 1–13, 2016.
[35] E. N. Bulgakov and D. N. Maksimov, "Light enhancement by quasi-bound states in the continuum in dielectric arrays," *Opt. Express*, vol. 25, no. 13, pp. 14 134–14 147, 2017.
[36] J. Gomis-Bresco, D. Artigas, and L. Torner, "Anisotropy-induced photonic bound states in the continuum," *Nature Photon.*, vol. 11, no. 4, pp. 232–236, 2017.
[37] Y. Plotnik *et al.*, "Experimental observation of optical bound states in the continuum," *Physical Rev. Lett.*, vol. 107, no. 18, 2011, Art. no. 183901.
[38] D. C. Marinica, A. G. Borisov, and S. V. Shabanov, "Bound states in the continuum in photonics," *Physical Rev. Lett.*, vol. 100, no. 18, 2008, Art. no. 183902.
[39] M. I. Molina, A. E. Miroshnichenko, and Y. S. Kivshar, "Surface bound states in the continuum," *Physical Rev. Lett.*, vol. 108, no. 7, 2012, Art. no. 070401.
[40] A. Kodigala, T. Lepetit, Q. Gu, B. Bahari, Y. Fainman, and B. Kanté, "Lasing action from photonic bound states in continuum," *Nature*, vol. 541, no. 7636, pp. 196–199, 2017.
[41] K. Hirose, Y. Liang, Y. Kurosaka, A. Watanabe, T. Sugiyama, and S. Noda, "Watt-class high-power, high-beam-quality photonic-crystal lasers," *Nature Photon.*, vol. 8, no. 5, pp. 406–411, 2014.
[42] K. Kitamura, K. Sakai, N. Takayama, M. Nishimoto, and S. Noda, "Focusing properties of vector vortex beams emitted by photonic-crystal lasers," *Opt. Lett.*, vol. 37, no. 12, pp. 2421–2423, 2012.
[43] J. Lee *et al.*, "Observation and differentiation of unique high-q optical resonances near zero wave vector in macroscopic photonic crystal slabs," *Physical Rev. Lett.*, vol. 109, no. 6, 2012, Art. no. 067401.
[44] C. W. Hsu *et al.*, "Observation of trapped light within the radiation continuum," *Nature*, vol. 499, no. 7457, pp. 188–191, 2013.
[45] J. Jin, X. Yin, L. Ni, M. Soljačić, B. Zhen, and C. Peng, "Topologically enabled ultrahigh-q guided resonances robust to out-of-plane scattering," *Nature*, vol. 574, no. 7779, pp. 501–504, 2019.
[46] H. M. Doeleman, F. Monticone, W. den Hollander, A. Alù, and A. F. Koenderink, "Experimental observation of a polarization vortex at an optical bound state in the continuum," *Nature Photon.*, vol. 12, no. 7, pp. 397–401, 2018.
[47] B. Zhen, C. W. Hsu, L. Lu, A. D. Stone, and M. Soljačć, "Topological nature of optical bound states in the continuum," *Physical Rev. Lett.*, vol. 113, no. 25, 2014, Art. no. 257401.